Three-Dimensional Lattice Boltzmann Model for High-Speed Compressible Flows

Feng Chen[1], Aiguo Xu[2*], Guangcai Zhang[2], Yingjun Li[1]

1, State Key Laboratory for GeoMechanics and Deep Underground Engineering, China University of Mining and Technology (Beijing), Beijing100083, China

2, National Key Laboratory of Computational Physics, Institute of Applied Physics and Computational Mathematics, P. O. Box 8009-26, Beijing 100088, P.R.China

(Dated: October 21, 2010)

Abstract

A highly efficient three-dimensional (3D) Lattice Boltzmann (LB) model for high speed compressible flows is proposed. This model is developed from the original one by Kataoka and Tsutahara[Phys. Rev. E 69, 056702 (2004)]. The convection term is discretized by the Non-oscillatory, containing No free parameters and Dissipative (NND) scheme, which effectively damps oscillations at discontinuities. To be more consistent with the kinetic theory of viscosity and to further improve the numerical stability, an additional dissipation term is introduced. Model parameters are chosen in such a way that the von Neumann stability criterion is satisfied. The new model is validated by well-known benchmarks, (i) Riemann problems, including the problem with Lax shock tube and a newly designed shock tube problem with high Mach number; (ii) reaction of shock wave on droplet or bubble. Good agreements are obtained between LB results and exact ones or previously reported solutions. The model is capable of simulating flows from subsonic to supersonic and capturing jumps resulted from shock waves.

PACS numbers: 47.11.-j, 51.10.+y, 05.20.Dd

Keywords: lattice Boltzmann method, compressible flows, Euler equations, von Neumann stability analysis

* Corresponding author. E-mail: Xu_Aiguo@iapcm.ac.cn

I. INTRODUCTION

Lattice Boltzmann (LB) method has been becoming a powerful and efficient tool to simulate fluid flows in many areas [1], ranging from multiphase flows [2, 3], magnetohydrodynamics [4–6], flows through porous media [7, 8] and thermal fluid dynamics [9]. However, most models so far work only for incompressible fluids. Many attempts have been made in constructing LB models for the compressible Euler equations. Hu et al. [10] proposed a 13-discrete-velocity model based on the triangular lattice. In this model, particles at each node are classified into three kinds. They are on the energy levels ϵ_A, ϵ_B, and ϵ_D, where $\epsilon_A > \epsilon_B > 0$, the energy level ϵ_D is higher than 0 and is for the rest particle. Similar to Hu's model, Yan and co-workers [11] presented a 17-discrete-velocity model with three-speed-three-energy level on a square lattice. Both models are two-dimensional (2D) and belong to the standard LB model. In the standard LB model, particle velocities are restricted to those exactly linking the lattice nodes in unit time. Besides the standard LB, Finite Difference (FD) LB is attracting more attention with time. With the FD LB model we do not need consider that constraint, we can choose particle velocities independently from the lattice configuration.

Shi et al. [12] formulated a FD LB scheme based on a two-dimensional 9-velocity model. This model allows particles to possess both kinetic and thermal energies. Kataoka and Tsutahara [13] presented a LB model series for the compressible Euler equations, where 5, 9 and 15 discrete velocities are used for the one- , two- and three-dimensional cases, respectively. However, all these models work only for subsonic flow. The low-Mach number constraint is generally related to the numerical stability problem. The latter has been partly addressed by a few potential solutions, for example, the entropic method [14], flux limiters [15], dissipation techniques [16–19] and multiple-relaxation-time LB approach [20].

Watari and Tsutahara proposed a three-dimensional FD LB model for Euler equations, where numerical simulations are successfully performed up to Mach number 1.7 [21]. But the number of discrete velocities in that model is up to 73, which is quite expensive from the view of computational side. Recently, a three-dimensional compressible FD LB model without free parameters was proposed [22], where 25 discrete velocities are used. With this model the momentum equations at the Navier-Stokes level and energy equation at the Euler level can be recovered. The maximum Mach number is 2.9 in simulations. Pan, et

al. [16] developed the 2D model by Kataoka and Tsutahara [13] by introducing reasonable dissipation term so that the model works for supersonic flows. Flows with Mach number higher than 30 are successfully simulated with the model.

In this paper we formulate a three-dimensional FD LB model for high speed compressible flows, based on Kataoka's 15-velocity model and reasonable dissipation technique. The following part of the paper is planned as follows. Section 2 presents the discrete velocity model used in this work. Section 3 describes briefly the FD scheme and performs the von Neumann stability analysis. Simulation results are presented and analyzed in Section 4. Section 5 makes the conclusion.

II. 3D DISCRETE VELOCITY MODEL BY KATAOKA AND TSUTAHARA

The evolution of the distribution function f_i is governed by the following equation [23]:

$$\frac{\partial f_i}{\partial t} + v_{i\alpha}\,\frac{\partial f_i}{\partial x_\alpha} = -\frac{1}{\tau}\left[f_i - f_i^{eq}\right], \tag{1}$$

where $v_{i\alpha}$ is the α component of velocity v_i, $i = 1, \ldots, N$, N is the number of discrete velocities, index $\alpha = 1,\ 2,\ 3$ corresponding to x, y, and z, respectively. The Einstein's convention for sums is used. The variable t is time, x_α is the spatial coordinate, f_i^{eq} is the local-equilibrium distribution function, and τ represents the relaxation time. At the continuous limit, the above formulation is required to recover the following Euler equations:

$$\begin{aligned}
\frac{\partial \rho}{\partial t} + \frac{\partial (\rho u_\alpha)}{\partial x_\alpha} &= 0, \\
\frac{\partial (\rho u_\alpha)}{\partial t} + \frac{\partial (\rho u_\alpha u_\beta)}{\partial x_\beta} + \frac{\partial P}{\partial x_\alpha} &= 0, \\
\frac{\partial \rho (bRT + u_\alpha^2)}{\partial t} + \frac{\partial \rho u_\alpha (bRT + u_\beta^2) + 2Pu_\alpha}{\partial x_\beta} &= 0,
\end{aligned} \tag{2}$$

where ρ, u_α, T, P are, respectively, the density, the flow velocity in the x_α direction, the temperature, and the pressure of gas. R is the specific gas constant and b is a constant relating to the specific-heat ratio γ, $b = 2/(\gamma - 1)$. The 3D discrete velocity model proposed by Kataoka and Tsutahara (see Fig. 1) can be expressed as:

$$(v_{i1}, v_{i2}, v_{i3}) = \begin{cases} (0,0,0) & \text{for } i = 1, \\ c_1\,(\pm 1, 0, 0)\,, c_1\,(0, \pm 1, 0)\,, c_1\,(0, 0, \pm 1) & \text{for } i = 2, 3, \cdots, 7, \\ \frac{c_2}{\sqrt{3}}\,(\pm 1, \pm 1, \pm 1) & \text{for } i = 8, 9, \cdots, 15, \end{cases}$$

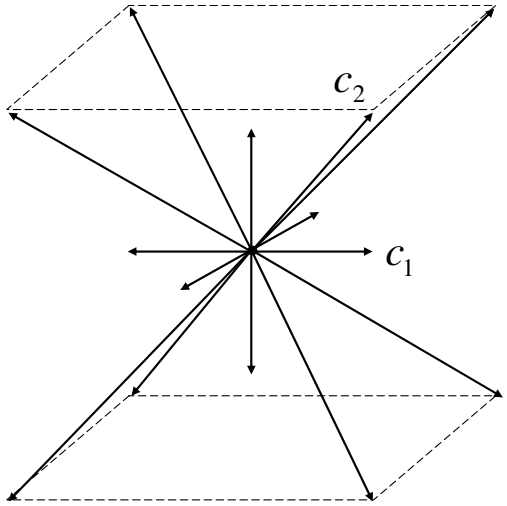

FIG. 1: Distribution of $\mathbf{v}_i$ for the proposed discrete velocity model.

$$\eta_i = \begin{cases} \eta_0, & \text{for } i = 1, \\ 0, & \text{for } i = 2, 3, \cdots, 15, \end{cases} \tag{3}$$

where c_1,c_2, and η_0 are given nonzero constants. In this model, the local-equilibrium distribution function f_i^{eq} satisfies the following relations:

$$\rho = \sum_{i=1}^{N} f_i^{eq}, \tag{4a}$$

$$\rho u_\alpha = \sum_{i=1}^{N} f_i^{eq} v_{i\alpha}, \tag{4b}$$

$$\rho(bRT + u_\alpha^2) = \sum_{i=1}^{N} f_i^{eq}(v_{i\alpha}^2 + \eta_i^2), \tag{4c}$$

$$P\delta_{\alpha\beta} + \rho u_\alpha u_\beta = \sum_{i=1}^{N} f_i^{eq} v_{i\alpha} v_{i\beta}, \tag{4d}$$

$$\rho[(b+2)RT + u_\beta^2]u_\alpha = \sum_{i=1}^{N} f_i^{eq}(v_{i\alpha}^2 + \eta_i^2) v_{i\alpha}. \tag{4e}$$

The local-equilibrium distribution function f_i^{eq} is defined as follows:

$$f_i^{eq} = \rho(A_i + B_i v_{i\alpha} u_\alpha + D_i u_\alpha v_{i\alpha} u_\beta v_{i\beta}),\ i = 1, 2, ..., 15, \tag{5}$$

where

$$A_i = \begin{cases} \frac{b-3}{\eta_0^2}T, & i=1 \\ \frac{1}{6(c_1^2-c_2^2)}\left[-c_2^2+\left((b-3)\frac{c_2^2}{\eta_0^2}+3\right)T+\frac{c_2^2}{c_1^2}u_\alpha^2\right], & i=2,3,\cdots,7 \\ \frac{1}{8(c_2^2-c_1^2)}\left[-c_1^2+\left((b-3)\frac{c_1^2}{\eta_0^2}+3\right)T+\frac{3c_1^2-c_2^2}{2c_2^2}u_\alpha^2\right], & i=8,9,\cdots,15 \end{cases}$$

$$B_i = \begin{cases} 0, & i=1 \\ \frac{-c_2^2+(b+2)T+u_\beta^2}{2c_1^2(c_1^2-c_2^2)}, & i=2,3,\cdots,7 \\ \frac{3[-c_1^2+(b+2)T+u_\beta^2]}{8c_2^2(c_2^2-c_1^2)}, & i=8,9,\cdots,15 \end{cases}, D_i = \begin{cases} 0, & i=1 \\ \frac{1}{2c_1^4}, & i=2,3,\cdots,7 \\ \frac{9}{16c_2^4}, & i=8,9,\cdots,15 \end{cases} \tag{6}$$

III. FD SCHEME AND VON NEUMANN STABILITY ANALYSIS

In the original LB model [13], the finite difference scheme with the first-order forward in time and the second-order upwind in space is used for the numerical computation. This model has been validated via the Riemann problem in subsonic flows and encounters instability problems in supersonic flows. In order to improve the stability, we adopt the Non-oscillatory, containing No free parameters and Dissipative (NND) scheme for space discretization. To be more consistent with the kinetic theory of viscosity and to further improve the numerical stability, an additional dissipation term is introduced.

In the NND scheme, the spacial derivative is calculated using the following formula:

$$\frac{\partial\left(v_{i\alpha}f_i\right)}{\partial x_\alpha} = \frac{1}{\triangle x_\alpha}\left(h_{i,I+\frac{1}{2}} - h_{i,I-\frac{1}{2}}\right), \tag{7}$$

where I represents node index in x or y direction. $h_{i,I+\frac{1}{2}}$ is the numerical flux at the interface of $\left(x_I+\frac{\Delta x}{2}, y\right)$ or $\left(x, y_I+\frac{\Delta y}{2}\right)$, and defined as:

$$h_{i,I+\frac{1}{2}} = f^L_{i,I+\frac{1}{2}} + f^R_{i,I+\frac{1}{2}}, \tag{8}$$

where

$$f^L_{i,I+\frac{1}{2}} = f^+_{i,I} + \frac{1}{2}\min\mathtt{mod}\left(\Delta f^+_{i,I+\frac{1}{2}}, \Delta f^+_{i,I-\frac{1}{2}}\right),$$

$$f^R_{i,I+\frac{1}{2}} = f^-_{i,I+1} - \frac{1}{2}\min\mathtt{mod}\left(\Delta f^-_{i,I+\frac{1}{2}}, \Delta f^-_{i,I+\frac{3}{2}}\right),$$

$$f^+_{i,I} = \frac{1}{2}\left(v_{i\alpha}+|v_{i\alpha}|\right)f_{i,I}, f^-_{i,I} = \frac{1}{2}\left(v_{i\alpha}-|v_{i\alpha}|\right)f_{i,I},$$

$$\Delta f^\pm_{i,I+\frac{1}{2}} = f^\pm_{i,I+1} - f^\pm_{i,I},$$

$$\min\mathtt{mod}\left(X,Y\right) = \frac{1}{2}\min\left(|X|,|Y|\right)\left[\mathtt{Sign}\left(X\right)+\mathtt{Sign}\left(Y\right)\right]. \tag{9}$$

The NND scheme itself contains a forth-order dissipation term with a negative coefficient which reduces the oscillations, but it is not enough to highly improve the stability, which means an additional dissipation term is needed for a practical LB simulation. In order to further improve the stability, and enhance its applicability for high Mach flows, we introduce artificial viscosity into the LB equation:

$$\frac{\partial f_i}{\partial t} + v_{i\alpha}\frac{\partial f_i}{\partial x_\alpha} = -\frac{1}{\tau}\left(f_i - f_i^{eq}\right) + \lambda_i \sum_{\alpha=1}^{3} \frac{\partial^2 f_i}{\partial x_\alpha^2}, \tag{10}$$

where

$$\lambda_i = \begin{cases} c_1\Delta x, & i = 1 \\ c_1\Delta x/10, & i = 2, 3, \cdots, 7 \\ 0, & i = 8, 9, \cdots, 15 \end{cases}.$$

The second-order derivative can be calculated by the central difference scheme.

In the following we do the von Neumann stability analysis of the improved LB model. In the stability analysis, we write the solution of FD LB equation in Fourier series form. If all the eigenvalues of the coefficient matrix are less than 1, the algorithm is stable.

Distribution function is split into two parts: $f_i(x_\alpha, t) = \bar{f_i^0} + \Delta f_i(x_\alpha, t)$, where $\bar{f_i^0}$ is the global equilibrium distribution function. It is a constant which does not change with time or space. Putting this equation into Eq. (10) we obtain:

$$\frac{\Delta f_i(x_\alpha, t+\Delta t) - \Delta f_i(x_\alpha, t)}{\Delta t} + v_{i\alpha}\frac{\partial f_i}{\partial x_\alpha} = -\frac{1}{\tau}\left(\Delta f_i - \Delta f_i^{eq}\right) + \lambda_i \frac{\partial^2 f_i}{\partial x_\alpha^2}, \tag{11}$$

the solution can be written as

$$\Delta f_i(x_\alpha, t) = F_i^t \exp(\mathbf{i} k_\alpha x_\alpha), \tag{12}$$

where F_i^t is an amplitude of sine wave at lattice point x_α and time t, k_α is the wave number. From the Eq.(11) and Eq.(12) we can get $F_i^{t+\Delta t} = G_{ij}F_j^t$. Coefficient matrix G_{ij} describes the growth rate of amplitude F_i^t in each time step Δt. The von Neumann stability condition is $\max|\omega| \leq 1$, where ω denotes the eigenvalue of coefficient matrix. Coefficient matrix G_{ij} of NND scheme can be expressed as follows,

$$G_{ij} = \left(1 - \frac{\Delta t}{\tau} - \frac{v_{i\alpha}\Delta t}{\Delta x_\alpha}\phi\right)\delta_{ij} + \frac{\Delta t}{\tau}\frac{\partial f_i^{eq}}{\partial f_j} + \lambda_i \Delta t \frac{(e^{\mathbf{i}k_\alpha \Delta x_\alpha} - 2 + e^{-\mathbf{i}k_\alpha \Delta x_\alpha})}{(\Delta x_\alpha)^2}\delta_{ij},$$

$$\phi = \begin{cases} (1-\widetilde{\alpha})\left(1 - e^{-\mathbf{i}k_\alpha \Delta x_\alpha}\right), & \text{if } v_{i\alpha} \geq 0; \\ \left(1 - \widetilde{\beta}\right)\left(e^{\mathbf{i}k_\alpha \Delta x_\alpha} - 1\right), & \text{if } v_{i\alpha} < 0. \end{cases}$$

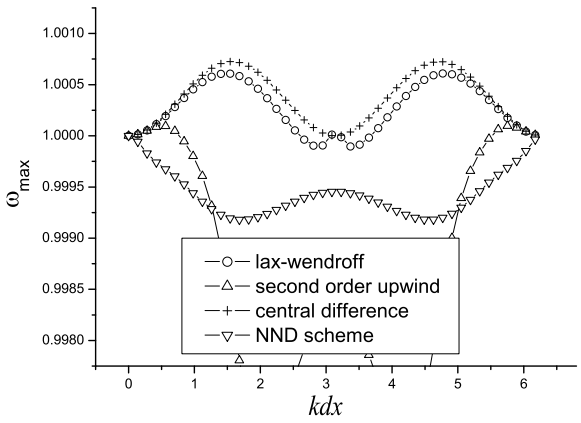

FIG. 2: Stability analysis of several finite difference schemes.

$$\frac{\partial f_i^{eq}}{\partial f_j} = \frac{\partial f_i^{eq}}{\partial \rho}\frac{\partial \rho}{\partial f_j} + \frac{\partial f_i^{eq}}{\partial T}\frac{\partial T}{\partial f_j} + \frac{\partial f_i^{eq}}{\partial u_\alpha}\frac{\partial u_\alpha}{\partial f_j}, |\widetilde{\alpha}| < \frac{1}{2}, \left|\widetilde{\beta}\right| < \frac{1}{2}. \tag{13}$$

There are some numerical results of von Neumann stability analysis by Mathematica. Abscissa is kdx, and ordinate is $|\omega|_{max}$ that is the biggest eigenvalue of coefficient matrix G_{ij}.

Figure 2 shows the stability analysis of several finite difference schemes. The macroscopic variables are set as $(\rho, u_1, u_2, u_3, T) = (1.0, 4.0, 0.0, 0.0, 1.0)$, the other model parameters are: $(c_1, c_2, \eta_0) = (4.0, 12.0, 4.0)$, $dx = dy = dz = 4 \times 10^{-3}$, $dt = \tau = 10^{-5}$, $b = 5$, $\widetilde{\alpha} = \widetilde{\beta} = 0$. In this test, the NND scheme shows better stability than the others. Figure 3 shows the effect of dissipation term. The variables are set as $(\rho, u_1, u_2, u_3, T) = (1.0, 20.0, 0.0, 0.0, 1.0)$, $(c_1, c_2, \eta_0) = (20.0, 60.0, 20.0)$, and the others are consistent with the Figure 2. In the two cases of Figure 3, operation with dissipation term is more stable($\max|\omega| \leq 1$).

Figure 4 shows the influence of parameters c_1, c_2, η_0 on the stability in the absence of dissipation term. The macroscopic variables and the other model parameters are consistent with those of Figure 2. Figure 5 shows the stability effect of the three parameters, when there is a dissipation term. The macroscopic variables and the other model parameters are consistent with those of Figure 3. In Figure 4 constants c_1, c_2 and η_0 affect the stability heavily. In Figure 5 the LB is stable for all tested values of c_2 and η_0. Based on these tests, we suggest that c_1 can be set a value close to the maximum of flow velocity, c_2 can be chosen about 3 times of the value of c_1, and η_0 can be set to be about $1 \sim 2$ times of the value of c_1.

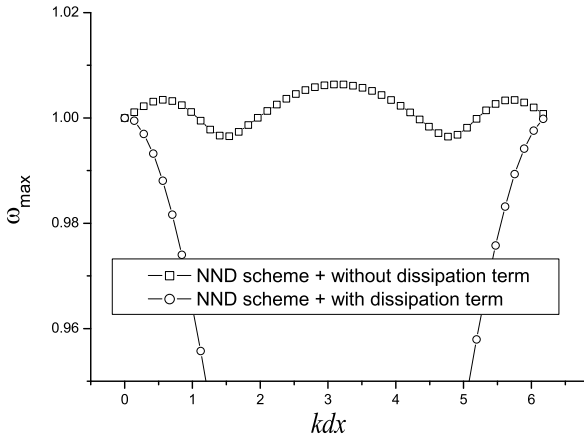

FIG. 3: Effect of dissipation term on numerical stability.

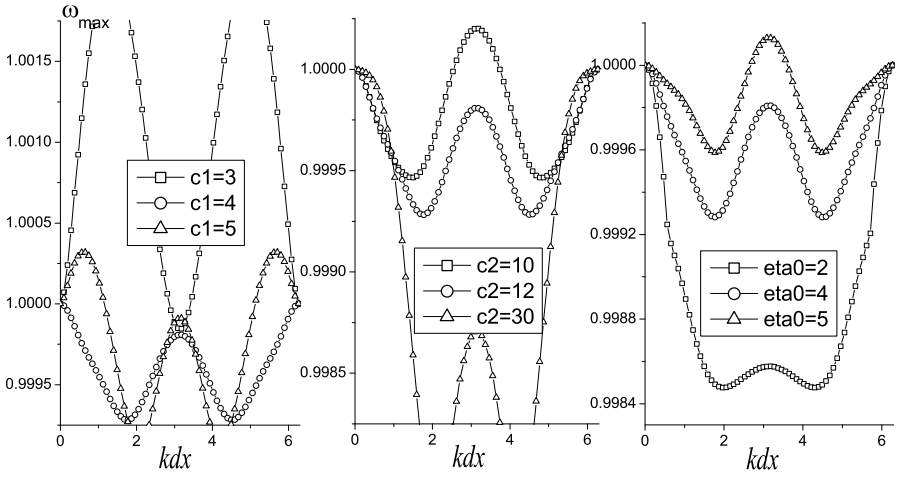

FIG. 4: Influence of parameters c_1, c_2, η_0 on stability in the absence of artificial viscosity.

IV. NUMERICAL SIMULATION AND ANALYSIS

In this section we study the following questions using the proposed LB model: one-dimensional Riemann problems, and reaction of shock wave on a droplet or bubble.

(1)One-dimensional Riemann problems

Here, we study two one-dimensional Riemann problems, including the problem with Lax shock tube and a newly designed shock tube problem with high Mach number. Subscripts "L" and "R" indicate the left and right macroscopic variables of discontinuity.

(a) Lax shock tube problem

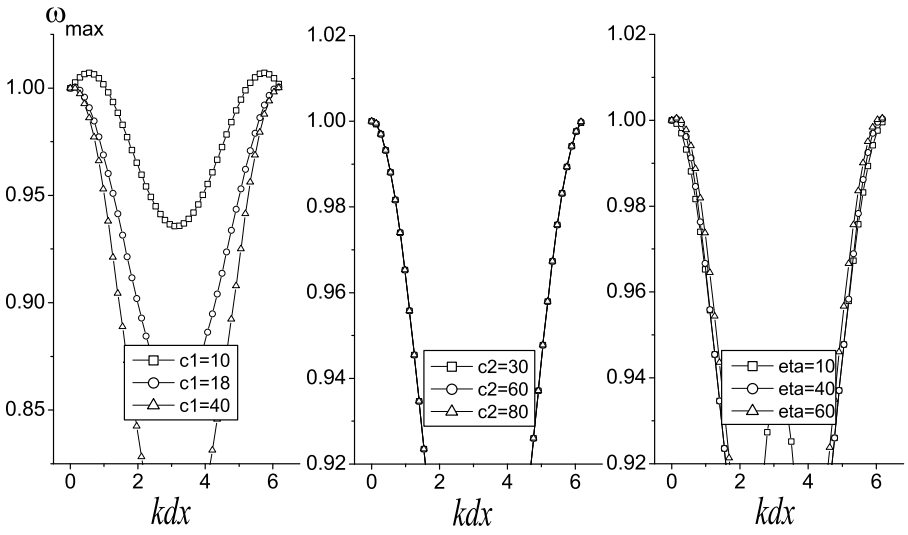

FIG. 5: Effect of c_1, c_2, η_0 under the condition with artificial viscosity term.

The initial condition of the problem can be defined:

$$\begin{aligned}(\rho, u_1, u_2, u_3, T)|_L &= (0.445, 0.698, 0.0, 0.0, 7.928),\\ (\rho, u_1, u_2, u_3, T)|_R &= (0.5, 0.0, 0.0, 0.0, 1.142).\end{aligned} \tag{14}$$

Figure 6 shows the comparison of the NND scheme and the second-order upwind scheme without the dissipation term at $t = 0.1$. Circles are for the NND scheme simulation results, squares correspond with the second-order upwind scheme, and solid lines are for exact solutions. The parameters are $(c_1, c_2, \eta_0) = (2.0, 6.0, 2.0)$, $\gamma = 1.4$, $dx = dy = dz = 0.003$, $dt = \tau = 10^{-5}$. Compared with the simulation results of second-order upwind scheme, the oscillations at the discontinuity are weaker in the NND simulation.

(b) High Mach number shock tube problem

In order to test the Mach number of the new model, we construct a new shock tube problem with high Mach number, and the initial condition is

$$\begin{aligned}(\rho, u_1, u_2, u_3, T)|_L &= (100.0, 10.0, 0.0, 0.0, 0.714286),\\ (\rho, u_1, u_2, u_3, T)|_R &= (150.0, 0.0, 0.0, 0.0, 50.0).\end{aligned} \tag{15}$$

Figure 7 shows a comparison of the numerical results and exact solutions at $t = 0.25$, where $(c_1, c_2, \eta_0) = (8.0, 24.0, 8.0)$, $\gamma = 1.4$, $dx = dy = dz = 0.01$, $dt = \tau = 10^{-5}$. The Mach number of the left side is 10 ($Ma = u/\sqrt{\gamma T} = 10/\sqrt{1.4 \times 0.714286}$), and the right is 0 ($Ma = u/\sqrt{\gamma T} = 0$). Successful simulation of this test shows the proposed model is still likely to have a high stability when the Mach number is large enough.

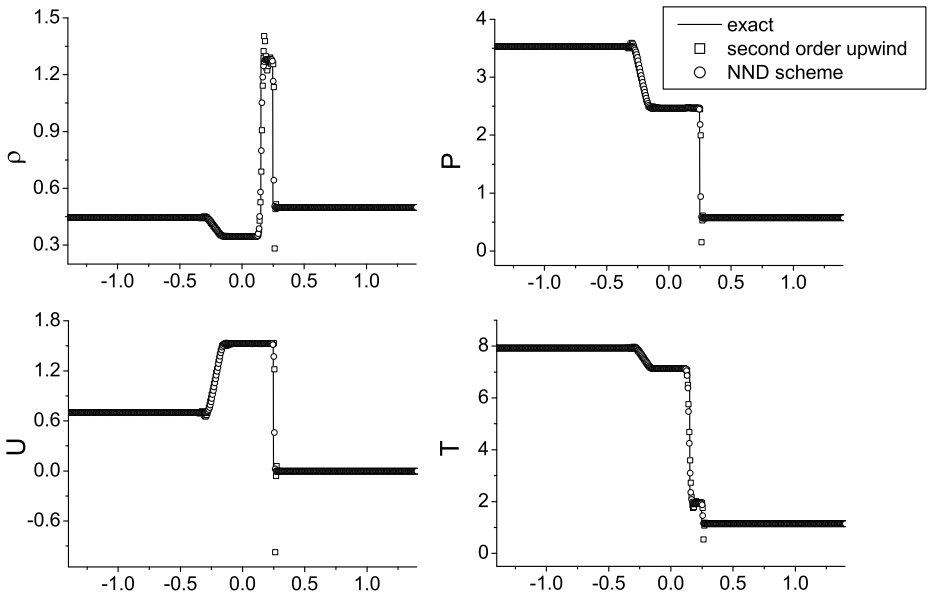

FIG. 6: Numerical results and exact solutions for Lax shock tube at $t = 0.1$.

(2) Reaction of shock wave on 3D bubble problem

The proposed model is used to simulate interaction of a planar shock wave with a bubble or droplet. The shock wave is moving from the right to the left. Initial conditions are (a)

$$(\rho, u_1, u_2, u_3, p)\mid_{x,y,0}= \begin{cases} (1,0,0,0,1), & \textbf{pre}-\textbf{shock}, \\ (2.66667,-1.47902,0,0,3.94406), & \textbf{post}-\textbf{shock}, \\ (0.1358,0,0,0,1), & \textbf{bubble}, \end{cases} \tag{16}$$

and (b)

$$(\rho, u_1, u_2, u_3, p)\mid_{x,y,0}= \begin{cases} (1,0,0,0,1), & \textbf{pre}-\textbf{shock}, \\ (2.66667,-1.47902,0,0,3.94406), & \textbf{post}-\textbf{shock}, \\ (4.1538,0,0,0,1), & \textbf{bubble}. \end{cases} \tag{17}$$

The corresponding shock wave Mach number is 2.0, $(Ma = (D-u)/\sqrt{\gamma T} = (2.36643 - 0)/\sqrt{1.4\times 1}$, where $D = 2.36643$ is the wavefront velocity).

The domain of computation is $(0:301, 0:81, 0:81)$. Initially, the bubble or droplet is at the position (200,40,40). In the simulations, the right side adopts the values of the initial post-shock flow, the extrapolation technique is applied at the left boundary, and reflection

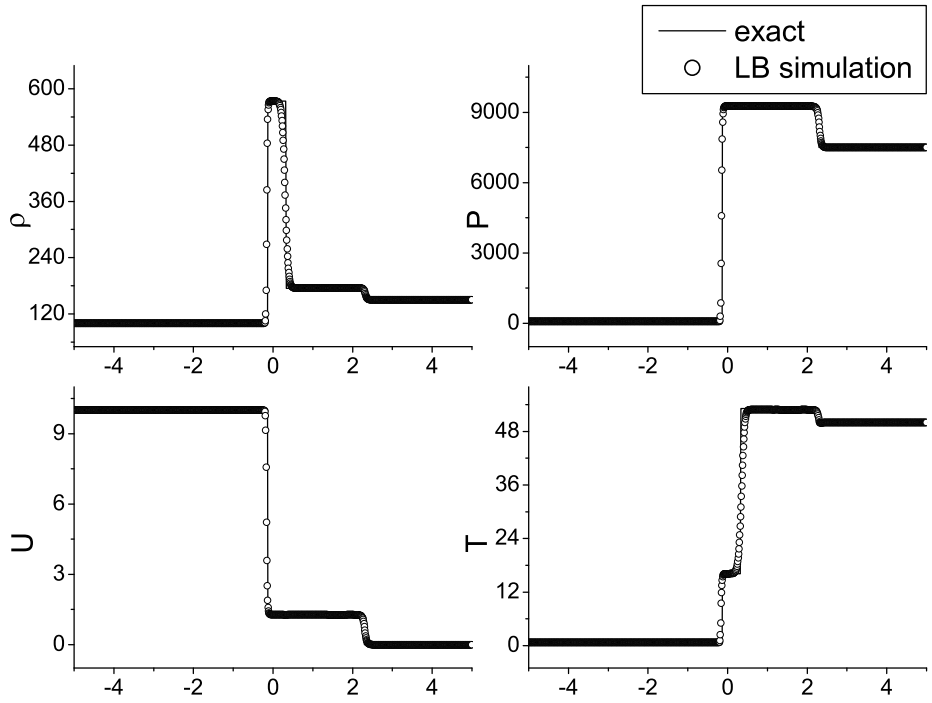

FIG. 7: The numerical and exact solutions for high Mach number shock tube at $t = 0.25$.

conditions are imposed on the other four surfaces. Specifically, at the right side,

$$\rho(NX+1, iy, iz) = \rho(NX, iy, iz) = 2.66667,$$
$$T(NX+1, iy, iz) = T(NX, iy, iz) = 1.6875,$$
$$u_1(NX+1, iy, iz) = u_1(NX, iy, iz) = -1.47902,$$
$$u_2(NX+1, iy, iz) = u_2(NX, iy, iz) = 0,$$
$$u_3(NX+1, iy, iz) = u_3(NX, iy, iz) = 0,$$

where ix (or iy, iz) is the index of lattice node in the x- (or y-, z-) direction, and $ix = 0$, $1, \cdots, NX+1$ ($iy = 0, 1, \cdots, NY+1$; $iz = 0, 1, \cdots, NZ+1$). At the left side $\rho(1, iy, iz) = 2\rho(2, iy, iz) - \rho(3, iy, iz)$, $\rho(0, iy, iz) = 2\rho(1, iy, iz) - \rho(2, iy, iz)$, temperature and velocity components have the same form. Finally we take the upper surface as an

example to describe the reflection conditions.

$$\begin{aligned}
\rho(ix, NY+1, iz) &= \rho(ix, NY-1, iz), \\
T(ix, NY+1, iz) &= T(ix, NY-1, iz), \\
u_1(ix, NY+1, iz) &= u_1(ix, NY-1, iz), \\
u_2(ix, NY+1, iz) &= -u_2(ix, NY-1, iz), \\
u_3(ix, NY+1, iz) &= u_3(ix, NY-1, iz),
\end{aligned}$$

$$\begin{aligned}
\rho(ix, NY, iz) &= \rho(ix, NY-1, iz), \\
T(ix, NY, iz) &= T(ix, NY-1, iz), \\
u_1(ix, NY, iz) &= u_1(ix, NY-1, iz), \\
u_2(ix, NY, iz) &= 0, \\
u_3(ix, NY, iz) &= u_3(ix, NY-1, iz).
\end{aligned}$$

Parameters are as follows: $(c_1, c_2, \eta_0) = (2.0, 6.0, 4.0)$, $\gamma = 1.4$, $dx = dy = dz = 0.001$, $dt = \tau = 10^{-5}$. Figure 8 and Figure 9 show the density iso-surfaces of bubble or droplet, where Figure 8 is for the process with initial condition (16), and Figure 9 is for condition (17). Figure 10 shows the density contours on section $z = 40$, where (a) and (b) correspond to the processes of Figure 8 and Figure 9, respectively. The simulation results are accordant with those by other numerical methods[24, 25] and experiment[26].

V. CONCLUSION

We proposed a highly efficient 3D LB model for high-speed compressible flows. The convection term in Boltzmann equation is solved with the finite difference NND method, additional dissipation term is introduced to match the more realistic kinetic viscosity and to be more stable in numerical simulations. Model parameters are controlled in such a way that the von Neumann stability criterion is satisfied. The model can be used to simulate flows from subsonic to supersonic flows, especially supersonic flows with shock waves.

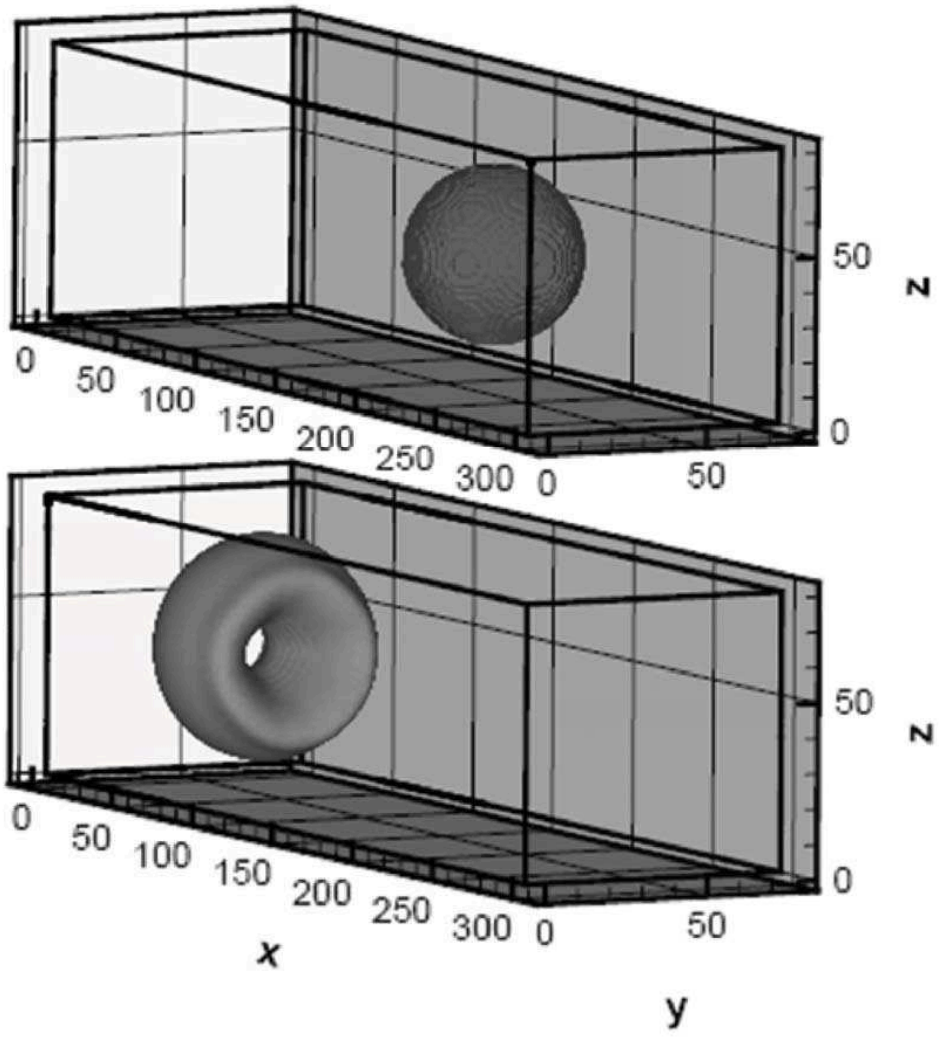

FIG. 8: Density iso-surfaces of a low density bubble at $t = 0.0$, 0.1, respectively.

Acknowledgments

This work is supported by the Science Foundations of LCP and CAEP [under Grant Nos. 2009A0102005, 2009B0101012], National Basic Research Program (973 Program) [under Grant No. 2007CB815105], National Natural Science Foundation [under Grant Nos. 10775018, 10702010,11075021,11074300] of China.

---

[1] S. Succi, *The Lattice Boltzmann Equation for Fluid Dynamics and Beyond,* Oxford University Press, New York(2001).

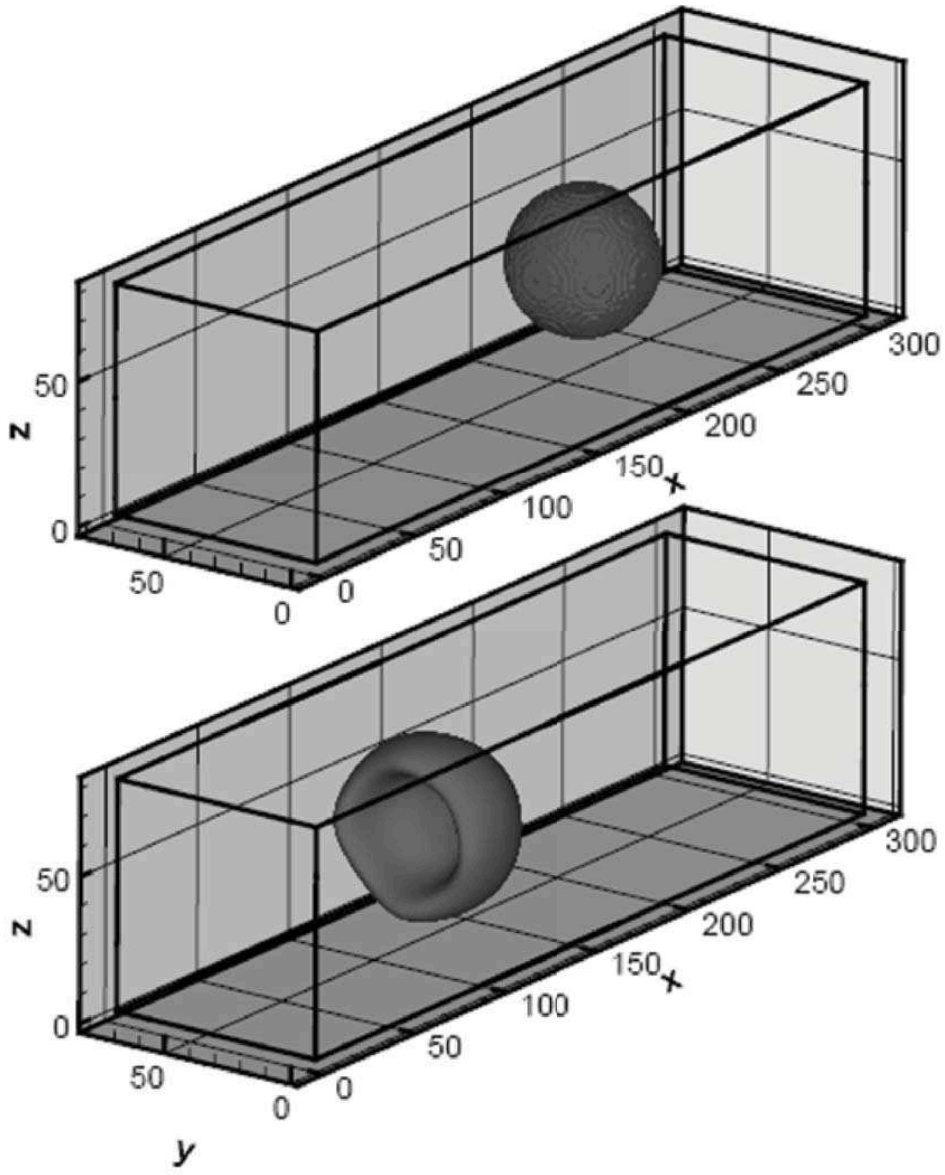

FIG. 9: Density iso-surfaces of a high density bubble at $t = 0.0$, 0.1, respectively.

[2] X. Shan, H. Chen, Phys. Rev. E **47** (1993) 1815; Phys. Rev. E **49** (1994) 2941.

[3] A.G. Xu, G. Gonnella, and A. Lamura, Phys. Rev. E **74** (2006) 011505; Phys. Rev. E **67** (2003) 056105; Physica A **331** (2004) 10; Physica A **344** (2004) 750; Physica A **362** (2006) 42; A.G. Xu, Commun. Theor. Phys. **39** (2003) 729.

[4] S.Chen, H.Chen, D.Martinez, and W.Matthaeus, Phys. Rev. Lett., **67** (1991) 3776.

[5] S.Succi, M.Vergassola and R.Benzi, Phys. Rev. A, **43** (1991) 4521.

[6] G.Breyiannis and D.Valougeorgis, Phys. Rev. E, **69** (2004) 065702(R).

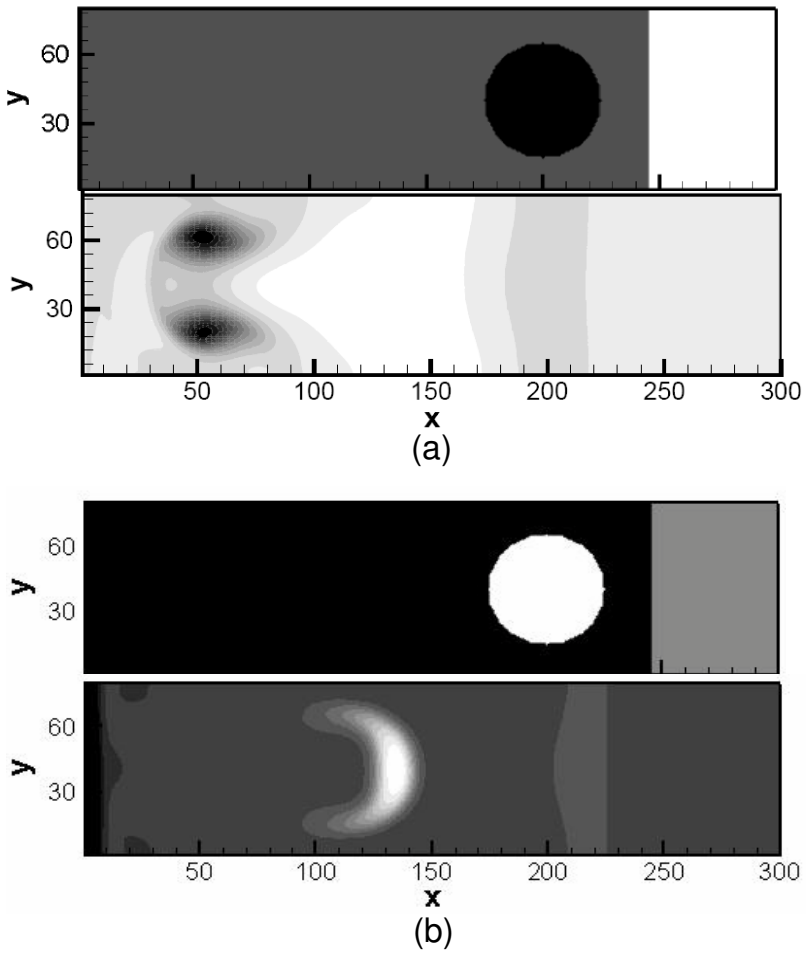

FIG. 10: Density contours on section $z = 40$ at $t = 0.0$, 0.1. (a) and (b) correspond to the processes of Figure 8 and Figure 9. From black to white, the density value increases.

[7] A. Gunstensen and D.H. Rothman, J. Geophy. Research **98** (1993) 6431.

[8] Q. J. Kang, D. X.Zhang, and S. Y.Chen, Phys. Rev. E, **66** (2002) 056307.

[9] Y. Chen, H. Ohashi, and M. Akiyama, J. Sci. Comp. **12** (1997) 169.

[10] S.X. Hu, G.W. Yan, W.P. Shi, Acta Mech. Sinica (English Series) **13** (1997) 218.

[11] G.W. Yan, Y.S. Chen, S.X. Hu, Phys. Rev. E **59** (1999) 454.

[12] W.P. Shi, W. Shyy, R. Mei, Numer. Heat Transfer, Part B **40** (2001) 1.

[13] T. Kataoka, M. Tsutahara, Phys. Rev. E **69** (2004) 056702.

[14] F. Tosi, S. Ubertini, S. Succi, H. Chen, I.V. Karlin, Math. Comput. Simul. **72** (2006) 227.

[15] V. Sofonea, A. Lamura, G. Gonnella, A. Cristea, Phys. Rev. E **70** (2004) 046702.

[16] X.F. Pan, A.G. Xu, G.C. Zhang, and S. Jiang, Int. J. Mod. Phys. C **18** (2007) 1747.

[17] Y.B. Gan, A.G. Xu, G.C. Zhang, X.J. Yu, and Y.J. Li, Physica A **387** (2008) 1721.

[18] F. Chen, A.G. Xu, G.C. Zhang, Y.B. Gan, T. Cheng, and Y.J. Li, Commun. Theor. Phys., **52** (2009) 681.

[19] R. A. Brownlee, A. N. Gorban, J. Levesley, Phys. Rev. E **75** (2007) 036711.

[20] F. Chen, A.G. Xu, G. C. Zhang, Y. J. Li and S. Succi, Europhys. Lett., (in press) [arXiv:1004.5442].

[21] M. Watari, M. Tsutahara, Physica A **364** (2006) 129.

[22] Q. Li, Y.L. He, Y. Wang, G.H. Tang, Physics Letters A **373** (2009) 2101.

[23] P. Bhatnagar, E. P. Gross, and M. K. Krook, Phys. Rev. **94** (1954) 511.

[24] C. Q. Jin, K. Xu. J. Comput. Phys. **218** (2006) 68.

[25] D. X. Fu, Y. W. Ma, X. L. Li, Chinese Phys. Lett. **25** (2008) 188.

[26] J. F. Haas, B. Sturtevant, J. Fluid Nech. **181** (1987) 41.

Three-Dimensional Lattice Boltzmann Model for High-Speed Compressible Flows

Feng Chen[1], Aiguo Xu[2*], Guangcai Zhang[2], Yingjun Li[1]

1, State Key Laboratory for GeoMechanics and Deep Underground Engineering, China University of Mining and Technology (Beijing), Beijing100083, China

2, National Key Laboratory of Computational Physics, Institute of Applied Physics and Computational Mathematics, P. O. Box 8009-26, Beijing 100088, P.R.China

(Dated: October 21, 2010)

Abstract

A highly efficient three-dimensional (3D) Lattice Boltzmann (LB) model for high speed compressible flows is proposed. This model is developed from the original one by Kataoka and Tsutahara[Phys. Rev. E 69, 056702 (2004)]. The convection term is discretized by the Non-oscillatory, containing No free parameters and Dissipative (NND) scheme, which effectively damps oscillations at discontinuities. To be more consistent with the kinetic theory of viscosity and to further improve the numerical stability, an additional dissipation term is introduced. Model parameters are chosen in such a way that the von Neumann stability criterion is satisfied. The new model is validated by well-known benchmarks, (i) Riemann problems, including the problem with Lax shock tube and a newly designed shock tube problem with high Mach number; (ii) reaction of shock wave on droplet or bubble. Good agreements are obtained between LB results and exact ones or previously reported solutions. The model is capable of simulating flows from subsonic to supersonic and capturing jumps resulted from shock waves.

PACS numbers: 47.11.-j, 51.10.+y, 05.20.Dd

Keywords: lattice Boltzmann method, compressible flows, Euler equations, von Neumann stability analysis

* Corresponding author. E-mail: Xu_Aiguo@iapcm.ac.cn

I. INTRODUCTION

Lattice Boltzmann (LB) method has been becoming a powerful and efficient tool to simulate fluid flows in many areas [1], ranging from multiphase flows [2, 3], magnetohydrodynamics [4–6], flows through porous media [7, 8] and thermal fluid dynamics [9]. However, most models so far work only for incompressible fluids. Many attempts have been made in constructing LB models for the compressible Euler equations. Hu et al. [10] proposed a 13-discrete-velocity model based on the triangular lattice. In this model, particles at each node are classified into three kinds. They are on the energy levels ϵ_A, ϵ_B, and ϵ_D, where $\epsilon_A > \epsilon_B > 0$, the energy level ϵ_D is higher than 0 and is for the rest particle. Similar to Hu's model, Yan and co-workers [11] presented a 17-discrete-velocity model with three-speed-three-energy level on a square lattice. Both models are two-dimensional (2D) and belong to the standard LB model. In the standard LB model, particle velocities are restricted to those exactly linking the lattice nodes in unit time. Besides the standard LB, Finite Difference (FD) LB is attracting more attention with time. With the FD LB model we do not need consider that constraint, we can choose particle velocities independently from the lattice configuration.

Shi et al. [12] formulated a FD LB scheme based on a two-dimensional 9-velocity model. This model allows particles to possess both kinetic and thermal energies. Kataoka and Tsutahara [13] presented a LB model series for the compressible Euler equations, where 5, 9 and 15 discrete velocities are used for the one- , two- and three-dimensional cases, respectively. However, all these models work only for subsonic flow. The low-Mach number constraint is generally related to the numerical stability problem. The latter has been partly addressed by a few potential solutions, for example, the entropic method [14], flux limiters [15], dissipation techniques [16–19] and multiple-relaxation-time LB approach [20].

Watari and Tsutahara proposed a three-dimensional FD LB model for Euler equations, where numerical simulations are successfully performed up to Mach number 1.7 [21]. But the number of discrete velocities in that model is up to 73, which is quite expensive from the view of computational side. Recently, a three-dimensional compressible FD LB model without free parameters was proposed [22], where 25 discrete velocities are used. With this model the momentum equations at the Navier-Stokes level and energy equation at the Euler level can be recovered. The maximum Mach number is 2.9 in simulations. Pan, et

al. [16] developed the 2D model by Kataoka and Tsutahara [13] by introducing reasonable dissipation term so that the model works for supersonic flows. Flows with Mach number higher than 30 are successfully simulated with the model.

In this paper we formulate a three-dimensional FD LB model for high speed compressible flows, based on Kataoka's 15-velocity model and reasonable dissipation technique. The following part of the paper is planned as follows. Section 2 presents the discrete velocity model used in this work. Section 3 describes briefly the FD scheme and performs the von Neumann stability analysis. Simulation results are presented and analyzed in Section 4. Section 5 makes the conclusion.

II. 3D DISCRETE VELOCITY MODEL BY KATAOKA AND TSUTAHARA

The evolution of the distribution function f_i is governed by the following equation [23]:

$$\frac{\partial f_i}{\partial t} + v_{i\alpha}\,\frac{\partial f_i}{\partial x_\alpha} = -\frac{1}{\tau}\left[f_i - f_i^{eq}\right], \tag{1}$$

where $v_{i\alpha}$ is the α component of velocity v_i, $i = 1, \ldots, N$, N is the number of discrete velocities, index $\alpha = 1,\ 2,\ 3$ corresponding to x, y, and z, respectively. The Einstein's convention for sums is used. The variable t is time, x_α is the spatial coordinate, f_i^{eq} is the local-equilibrium distribution function, and τ represents the relaxation time. At the continuous limit, the above formulation is required to recover the following Euler equations:

$$\begin{aligned}
\frac{\partial \rho}{\partial t} + \frac{\partial (\rho u_\alpha)}{\partial x_\alpha} &= 0, \\
\frac{\partial (\rho u_\alpha)}{\partial t} + \frac{\partial (\rho u_\alpha u_\beta)}{\partial x_\beta} + \frac{\partial P}{\partial x_\alpha} &= 0, \\
\frac{\partial \rho (bRT + u_\alpha^2)}{\partial t} + \frac{\partial \rho u_\alpha (bRT + u_\beta^2) + 2Pu_\alpha}{\partial x_\beta} &= 0,
\end{aligned} \tag{2}$$

where ρ, u_α, T, P are, respectively, the density, the flow velocity in the x_α direction, the temperature, and the pressure of gas. R is the specific gas constant and b is a constant relating to the specific-heat ratio γ, $b = 2/(\gamma - 1)$. The 3D discrete velocity model proposed by Kataoka and Tsutahara (see Fig. 1) can be expressed as:

$$(v_{i1}, v_{i2}, v_{i3}) = \begin{cases} (0,0,0) & \text{for } i = 1, \\ c_1\,(\pm 1, 0, 0)\,, c_1\,(0, \pm 1, 0)\,, c_1\,(0, 0, \pm 1) & \text{for } i = 2, 3, \cdots, 7, \\ \frac{c_2}{\sqrt{3}}\,(\pm 1, \pm 1, \pm 1) & \text{for } i = 8, 9, \cdots, 15, \end{cases}$$

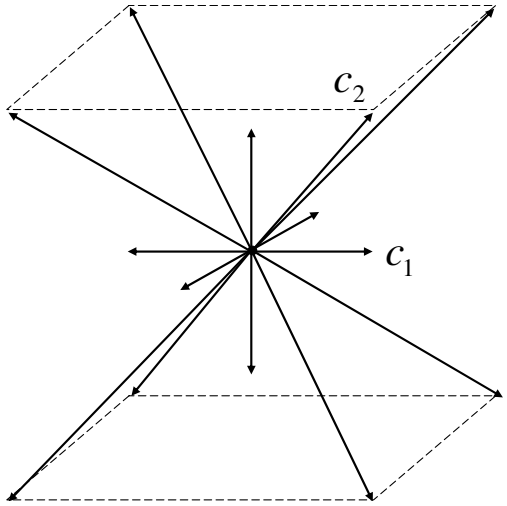

FIG. 1: Distribution of $\mathbf{v}_i$ for the proposed discrete velocity model.

$$\eta_i = \begin{cases} \eta_0, & \text{for } i = 1, \\ 0, & \text{for } i = 2, 3, \cdots, 15, \end{cases} \tag{3}$$

where c_1,c_2, and η_0 are given nonzero constants. In this model, the local-equilibrium distribution function f_i^{eq} satisfies the following relations:

$$\rho = \sum_{i=1}^{N} f_i^{eq}, \tag{4a}$$

$$\rho u_\alpha = \sum_{i=1}^{N} f_i^{eq} v_{i\alpha}, \tag{4b}$$

$$\rho(bRT + u_\alpha^2) = \sum_{i=1}^{N} f_i^{eq}(v_{i\alpha}^2 + \eta_i^2), \tag{4c}$$

$$P\delta_{\alpha\beta} + \rho u_\alpha u_\beta = \sum_{i=1}^{N} f_i^{eq} v_{i\alpha} v_{i\beta}, \tag{4d}$$

$$\rho[(b+2)RT + u_\beta^2]u_\alpha = \sum_{i=1}^{N} f_i^{eq}(v_{i\alpha}^2 + \eta_i^2) v_{i\alpha}. \tag{4e}$$

The local-equilibrium distribution function f_i^{eq} is defined as follows:

$$f_i^{eq} = \rho(A_i + B_i v_{i\alpha} u_\alpha + D_i u_\alpha v_{i\alpha} u_\beta v_{i\beta}),\ i = 1, 2, ..., 15, \tag{5}$$

where

$$A_i = \begin{cases} \frac{b-3}{\eta_0^2}T, & i=1 \\ \frac{1}{6(c_1^2-c_2^2)}\left[-c_2^2+\left((b-3)\frac{c_2^2}{\eta_0^2}+3\right)T+\frac{c_2^2}{c_1^2}u_\alpha^2\right], & i=2,3,\cdots,7 \\ \frac{1}{8(c_2^2-c_1^2)}\left[-c_1^2+\left((b-3)\frac{c_1^2}{\eta_0^2}+3\right)T+\frac{3c_1^2-c_2^2}{2c_2^2}u_\alpha^2\right], & i=8,9,\cdots,15 \end{cases}$$

$$B_i = \begin{cases} 0, & i=1 \\ \frac{-c_2^2+(b+2)T+u_\beta^2}{2c_1^2(c_1^2-c_2^2)}, & i=2,3,\cdots,7 \\ \frac{3[-c_1^2+(b+2)T+u_\beta^2]}{8c_2^2(c_2^2-c_1^2)}, & i=8,9,\cdots,15 \end{cases}, D_i = \begin{cases} 0, & i=1 \\ \frac{1}{2c_1^4}, & i=2,3,\cdots,7 \\ \frac{9}{16c_2^4}, & i=8,9,\cdots,15 \end{cases} \tag{6}$$

III. FD SCHEME AND VON NEUMANN STABILITY ANALYSIS

In the original LB model [13], the finite difference scheme with the first-order forward in time and the second-order upwind in space is used for the numerical computation. This model has been validated via the Riemann problem in subsonic flows and encounters instability problems in supersonic flows. In order to improve the stability, we adopt the Non-oscillatory, containing No free parameters and Dissipative (NND) scheme for space discretization. To be more consistent with the kinetic theory of viscosity and to further improve the numerical stability, an additional dissipation term is introduced.

In the NND scheme, the spacial derivative is calculated using the following formula:

$$\frac{\partial\left(v_{i\alpha}f_i\right)}{\partial x_\alpha} = \frac{1}{\triangle x_\alpha}\left(h_{i,I+\frac{1}{2}} - h_{i,I-\frac{1}{2}}\right), \tag{7}$$

where I represents node index in x or y direction. $h_{i,I+\frac{1}{2}}$ is the numerical flux at the interface of $\left(x_I+\frac{\Delta x}{2}, y\right)$ or $\left(x, y_I+\frac{\Delta y}{2}\right)$, and defined as:

$$h_{i,I+\frac{1}{2}} = f^L_{i,I+\frac{1}{2}} + f^R_{i,I+\frac{1}{2}}, \tag{8}$$

where

$$f^L_{i,I+\frac{1}{2}} = f^+_{i,I} + \frac{1}{2}\min\mathtt{mod}\left(\Delta f^+_{i,I+\frac{1}{2}}, \Delta f^+_{i,I-\frac{1}{2}}\right),$$

$$f^R_{i,I+\frac{1}{2}} = f^-_{i,I+1} - \frac{1}{2}\min\mathtt{mod}\left(\Delta f^-_{i,I+\frac{1}{2}}, \Delta f^-_{i,I+\frac{3}{2}}\right),$$

$$f^+_{i,I} = \frac{1}{2}\left(v_{i\alpha}+|v_{i\alpha}|\right)f_{i,I}, f^-_{i,I} = \frac{1}{2}\left(v_{i\alpha}-|v_{i\alpha}|\right)f_{i,I},$$

$$\Delta f^\pm_{i,I+\frac{1}{2}} = f^\pm_{i,I+1} - f^\pm_{i,I},$$

$$\min\mathtt{mod}\left(X,Y\right) = \frac{1}{2}\min\left(|X|,|Y|\right)\left[\mathtt{Sign}\left(X\right)+\mathtt{Sign}\left(Y\right)\right]. \tag{9}$$

The NND scheme itself contains a forth-order dissipation term with a negative coefficient which reduces the oscillations, but it is not enough to highly improve the stability, which means an additional dissipation term is needed for a practical LB simulation. In order to further improve the stability, and enhance its applicability for high Mach flows, we introduce artificial viscosity into the LB equation:

$$\frac{\partial f_i}{\partial t} + v_{i\alpha}\frac{\partial f_i}{\partial x_\alpha} = -\frac{1}{\tau}\left(f_i - f_i^{eq}\right) + \lambda_i \sum_{\alpha=1}^{3} \frac{\partial^2 f_i}{\partial x_\alpha^2}, \tag{10}$$

where

$$\lambda_i = \begin{cases} c_1\Delta x, & i = 1 \\ c_1\Delta x/10, & i = 2, 3, \cdots, 7 \\ 0, & i = 8, 9, \cdots, 15 \end{cases}.$$

The second-order derivative can be calculated by the central difference scheme.

In the following we do the von Neumann stability analysis of the improved LB model. In the stability analysis, we write the solution of FD LB equation in Fourier series form. If all the eigenvalues of the coefficient matrix are less than 1, the algorithm is stable.

Distribution function is split into two parts: $f_i(x_\alpha, t) = \bar{f_i^0} + \Delta f_i(x_\alpha, t)$, where $\bar{f_i^0}$ is the global equilibrium distribution function. It is a constant which does not change with time or space. Putting this equation into Eq. (10) we obtain:

$$\frac{\Delta f_i(x_\alpha, t+\Delta t) - \Delta f_i(x_\alpha, t)}{\Delta t} + v_{i\alpha}\frac{\partial f_i}{\partial x_\alpha} = -\frac{1}{\tau}\left(\Delta f_i - \Delta f_i^{eq}\right) + \lambda_i \frac{\partial^2 f_i}{\partial x_\alpha^2}, \tag{11}$$

the solution can be written as

$$\Delta f_i(x_\alpha, t) = F_i^t \exp(\mathbf{i} k_\alpha x_\alpha), \tag{12}$$

where F_i^t is an amplitude of sine wave at lattice point x_α and time t, k_α is the wave number. From the Eq.(11) and Eq.(12) we can get $F_i^{t+\Delta t} = G_{ij}F_j^t$. Coefficient matrix G_{ij} describes the growth rate of amplitude F_i^t in each time step Δt. The von Neumann stability condition is $\max|\omega| \leq 1$, where ω denotes the eigenvalue of coefficient matrix. Coefficient matrix G_{ij} of NND scheme can be expressed as follows,

$$G_{ij} = \left(1 - \frac{\Delta t}{\tau} - \frac{v_{i\alpha}\Delta t}{\Delta x_\alpha}\phi\right)\delta_{ij} + \frac{\Delta t}{\tau}\frac{\partial f_i^{eq}}{\partial f_j} + \lambda_i \Delta t \frac{(e^{\mathbf{i}k_\alpha \Delta x_\alpha} - 2 + e^{-\mathbf{i}k_\alpha \Delta x_\alpha})}{(\Delta x_\alpha)^2}\delta_{ij},$$

$$\phi = \begin{cases} (1-\widetilde{\alpha})\left(1 - e^{-\mathbf{i}k_\alpha \Delta x_\alpha}\right), & \text{if } v_{i\alpha} \geq 0; \\ \left(1 - \widetilde{\beta}\right)\left(e^{\mathbf{i}k_\alpha \Delta x_\alpha} - 1\right), & \text{if } v_{i\alpha} < 0. \end{cases}$$

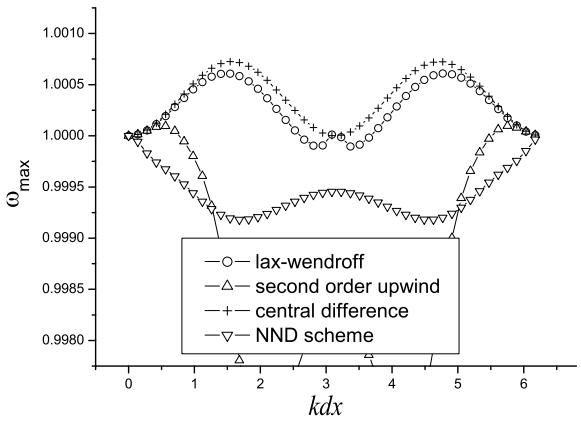

FIG. 2: Stability analysis of several finite difference schemes.

$$\frac{\partial f_i^{eq}}{\partial f_j} = \frac{\partial f_i^{eq}}{\partial \rho}\frac{\partial \rho}{\partial f_j} + \frac{\partial f_i^{eq}}{\partial T}\frac{\partial T}{\partial f_j} + \frac{\partial f_i^{eq}}{\partial u_\alpha}\frac{\partial u_\alpha}{\partial f_j}, |\widetilde{\alpha}| < \frac{1}{2}, \left|\widetilde{\beta}\right| < \frac{1}{2}. \tag{13}$$

There are some numerical results of von Neumann stability analysis by Mathematica. Abscissa is kdx, and ordinate is $|\omega|_{max}$ that is the biggest eigenvalue of coefficient matrix G_{ij}.

Figure 2 shows the stability analysis of several finite difference schemes. The macroscopic variables are set as $(\rho, u_1, u_2, u_3, T) = (1.0, 4.0, 0.0, 0.0, 1.0)$, the other model parameters are: $(c_1, c_2, \eta_0) = (4.0, 12.0, 4.0)$, $dx = dy = dz = 4 \times 10^{-3}$, $dt = \tau = 10^{-5}$, $b = 5$, $\widetilde{\alpha} = \widetilde{\beta} = 0$. In this test, the NND scheme shows better stability than the others. Figure 3 shows the effect of dissipation term. The variables are set as $(\rho, u_1, u_2, u_3, T) = (1.0, 20.0, 0.0, 0.0, 1.0)$, $(c_1, c_2, \eta_0) = (20.0, 60.0, 20.0)$, and the others are consistent with the Figure 2. In the two cases of Figure 3, operation with dissipation term is more stable($\max|\omega| \leq 1$).

Figure 4 shows the influence of parameters c_1, c_2, η_0 on the stability in the absence of dissipation term. The macroscopic variables and the other model parameters are consistent with those of Figure 2. Figure 5 shows the stability effect of the three parameters, when there is a dissipation term. The macroscopic variables and the other model parameters are consistent with those of Figure 3. In Figure 4 constants c_1, c_2 and η_0 affect the stability heavily. In Figure 5 the LB is stable for all tested values of c_2 and η_0. Based on these tests, we suggest that c_1 can be set a value close to the maximum of flow velocity, c_2 can be chosen about 3 times of the value of c_1, and η_0 can be set to be about $1 \sim 2$ times of the value of c_1.

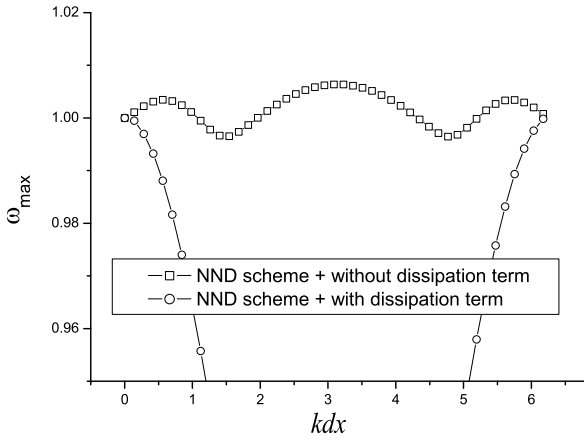

FIG. 3: Effect of dissipation term on numerical stability.

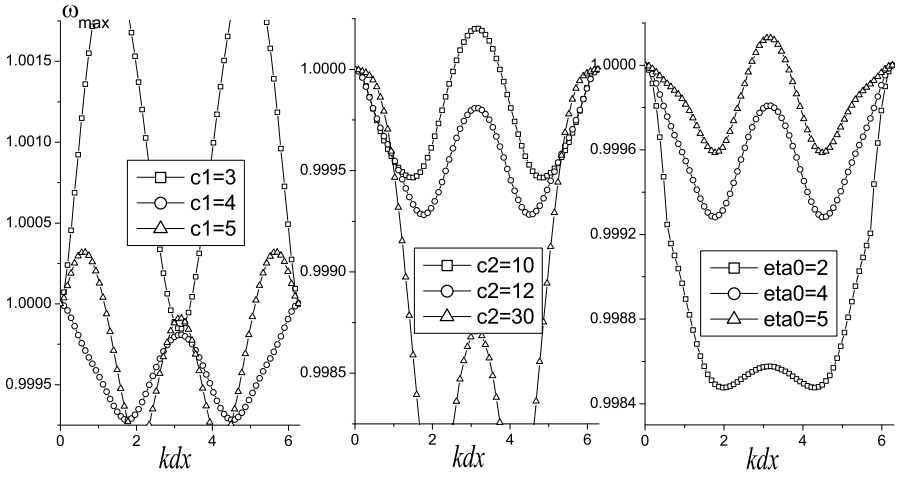

FIG. 4: Influence of parameters c_1, c_2, η_0 on stability in the absence of artificial viscosity.

IV. NUMERICAL SIMULATION AND ANALYSIS

In this section we study the following questions using the proposed LB model: one-dimensional Riemann problems, and reaction of shock wave on a droplet or bubble.

(1)One-dimensional Riemann problems

Here, we study two one-dimensional Riemann problems, including the problem with Lax shock tube and a newly designed shock tube problem with high Mach number. Subscripts "L" and "R" indicate the left and right macroscopic variables of discontinuity.

(a) Lax shock tube problem

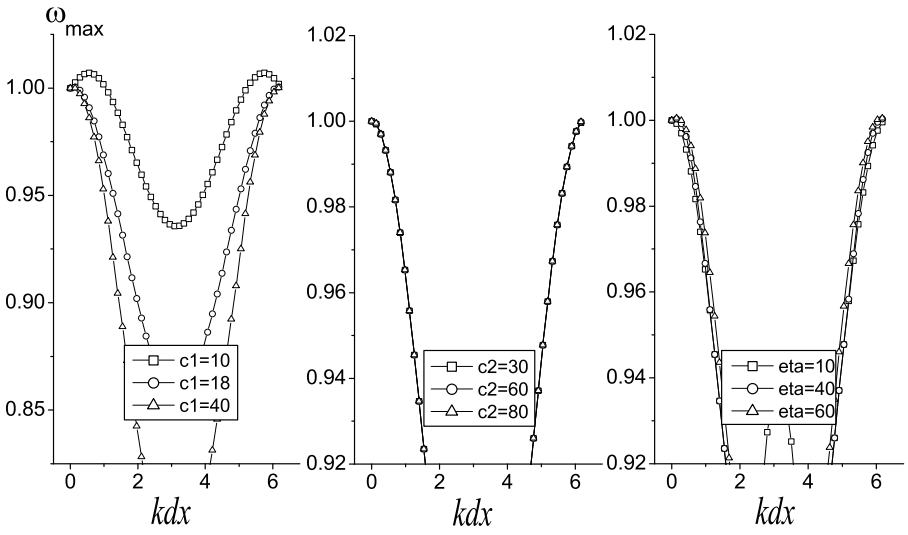

FIG. 5: Effect of c_1, c_2, η_0 under the condition with artificial viscosity term.

The initial condition of the problem can be defined:

$$\begin{aligned}(\rho, u_1, u_2, u_3, T)|_L &= (0.445, 0.698, 0.0, 0.0, 7.928),\\ (\rho, u_1, u_2, u_3, T)|_R &= (0.5, 0.0, 0.0, 0.0, 1.142).\end{aligned} \tag{14}$$

Figure 6 shows the comparison of the NND scheme and the second-order upwind scheme without the dissipation term at $t = 0.1$. Circles are for the NND scheme simulation results, squares correspond with the second-order upwind scheme, and solid lines are for exact solutions. The parameters are $(c_1, c_2, \eta_0) = (2.0, 6.0, 2.0)$, $\gamma = 1.4$, $dx = dy = dz = 0.003$, $dt = \tau = 10^{-5}$. Compared with the simulation results of second-order upwind scheme, the oscillations at the discontinuity are weaker in the NND simulation.

(b) High Mach number shock tube problem

In order to test the Mach number of the new model, we construct a new shock tube problem with high Mach number, and the initial condition is

$$\begin{aligned}(\rho, u_1, u_2, u_3, T)|_L &= (100.0, 10.0, 0.0, 0.0, 0.714286),\\ (\rho, u_1, u_2, u_3, T)|_R &= (150.0, 0.0, 0.0, 0.0, 50.0).\end{aligned} \tag{15}$$

Figure 7 shows a comparison of the numerical results and exact solutions at $t = 0.25$, where $(c_1, c_2, \eta_0) = (8.0, 24.0, 8.0)$, $\gamma = 1.4$, $dx = dy = dz = 0.01$, $dt = \tau = 10^{-5}$. The Mach number of the left side is 10 ($Ma = u/\sqrt{\gamma T} = 10/\sqrt{1.4 \times 0.714286}$), and the right is 0 ($Ma = u/\sqrt{\gamma T} = 0$). Successful simulation of this test shows the proposed model is still likely to have a high stability when the Mach number is large enough.

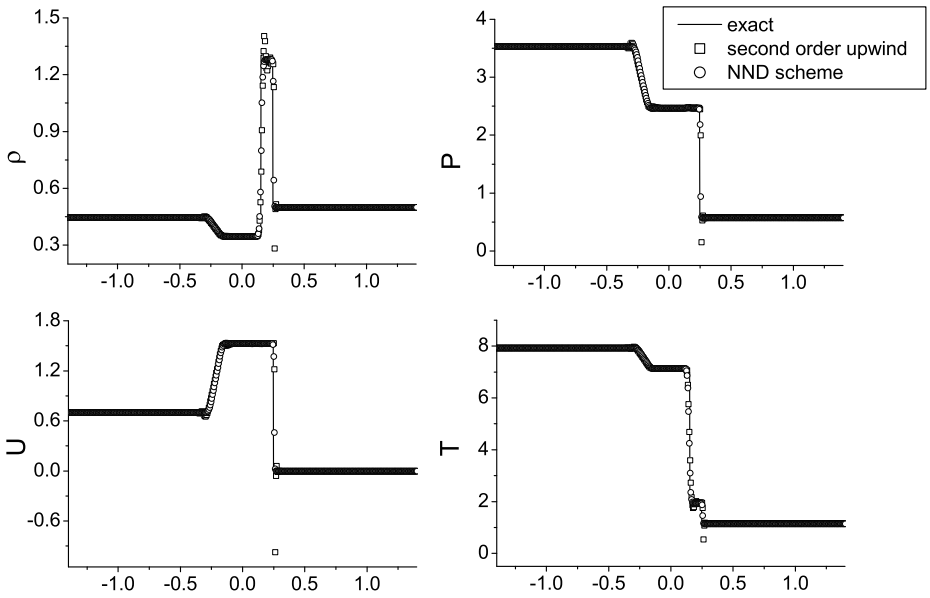

FIG. 6: Numerical results and exact solutions for Lax shock tube at $t = 0.1$.

(2) Reaction of shock wave on 3D bubble problem

The proposed model is used to simulate interaction of a planar shock wave with a bubble or droplet. The shock wave is moving from the right to the left. Initial conditions are (a)

$$(\rho, u_1, u_2, u_3, p)\mid_{x,y,0}= \begin{cases} (1,0,0,0,1), & \textbf{pre}-\textbf{shock}, \\ (2.66667,-1.47902,0,0,3.94406), & \textbf{post}-\textbf{shock}, \\ (0.1358,0,0,0,1), & \textbf{bubble}, \end{cases} \tag{16}$$

and (b)

$$(\rho, u_1, u_2, u_3, p)\mid_{x,y,0}= \begin{cases} (1,0,0,0,1), & \textbf{pre}-\textbf{shock}, \\ (2.66667,-1.47902,0,0,3.94406), & \textbf{post}-\textbf{shock}, \\ (4.1538,0,0,0,1), & \textbf{bubble}. \end{cases} \tag{17}$$

The corresponding shock wave Mach number is 2.0, $(Ma = (D-u)/\sqrt{\gamma T} = (2.36643 - 0)/\sqrt{1.4\times 1}$, where $D = 2.36643$ is the wavefront velocity).

The domain of computation is $(0:301, 0:81, 0:81)$. Initially, the bubble or droplet is at the position (200,40,40). In the simulations, the right side adopts the values of the initial post-shock flow, the extrapolation technique is applied at the left boundary, and reflection

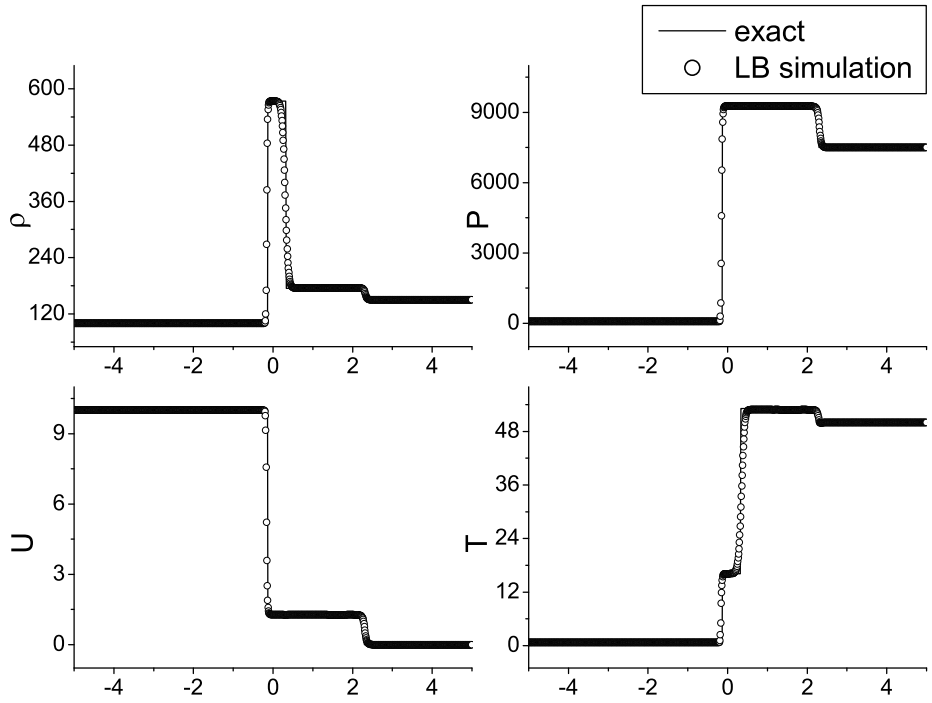

FIG. 7: The numerical and exact solutions for high Mach number shock tube at $t = 0.25$.

conditions are imposed on the other four surfaces. Specifically, at the right side,

$$\rho(NX+1, iy, iz) = \rho(NX, iy, iz) = 2.66667,$$
$$T(NX+1, iy, iz) = T(NX, iy, iz) = 1.6875,$$
$$u_1(NX+1, iy, iz) = u_1(NX, iy, iz) = -1.47902,$$
$$u_2(NX+1, iy, iz) = u_2(NX, iy, iz) = 0,$$
$$u_3(NX+1, iy, iz) = u_3(NX, iy, iz) = 0,$$

where ix (or iy, iz) is the index of lattice node in the x- (or y-, z-) direction, and $ix = 0$, $1, \cdots, NX+1$ ($iy = 0, 1, \cdots, NY+1$; $iz = 0, 1, \cdots, NZ+1$). At the left side $\rho(1, iy, iz) = 2\rho(2, iy, iz) - \rho(3, iy, iz)$, $\rho(0, iy, iz) = 2\rho(1, iy, iz) - \rho(2, iy, iz)$, temperature and velocity components have the same form. Finally we take the upper surface as an

example to describe the reflection conditions.

$$\begin{aligned}
\rho(ix, NY+1, iz) &= \rho(ix, NY-1, iz), \\
T(ix, NY+1, iz) &= T(ix, NY-1, iz), \\
u_1(ix, NY+1, iz) &= u_1(ix, NY-1, iz), \\
u_2(ix, NY+1, iz) &= -u_2(ix, NY-1, iz), \\
u_3(ix, NY+1, iz) &= u_3(ix, NY-1, iz),
\end{aligned}$$

$$\begin{aligned}
\rho(ix, NY, iz) &= \rho(ix, NY-1, iz), \\
T(ix, NY, iz) &= T(ix, NY-1, iz), \\
u_1(ix, NY, iz) &= u_1(ix, NY-1, iz), \\
u_2(ix, NY, iz) &= 0, \\
u_3(ix, NY, iz) &= u_3(ix, NY-1, iz).
\end{aligned}$$

Parameters are as follows: $(c_1, c_2, \eta_0) = (2.0, 6.0, 4.0)$, $\gamma = 1.4$, $dx = dy = dz = 0.001$, $dt = \tau = 10^{-5}$. Figure 8 and Figure 9 show the density iso-surfaces of bubble or droplet, where Figure 8 is for the process with initial condition (16), and Figure 9 is for condition (17). Figure 10 shows the density contours on section $z = 40$, where (a) and (b) correspond to the processes of Figure 8 and Figure 9, respectively. The simulation results are accordant with those by other numerical methods[24, 25] and experiment[26].

V. CONCLUSION

We proposed a highly efficient 3D LB model for high-speed compressible flows. The convection term in Boltzmann equation is solved with the finite difference NND method, additional dissipation term is introduced to match the more realistic kinetic viscosity and to be more stable in numerical simulations. Model parameters are controlled in such a way that the von Neumann stability criterion is satisfied. The model can be used to simulate flows from subsonic to supersonic flows, especially supersonic flows with shock waves.

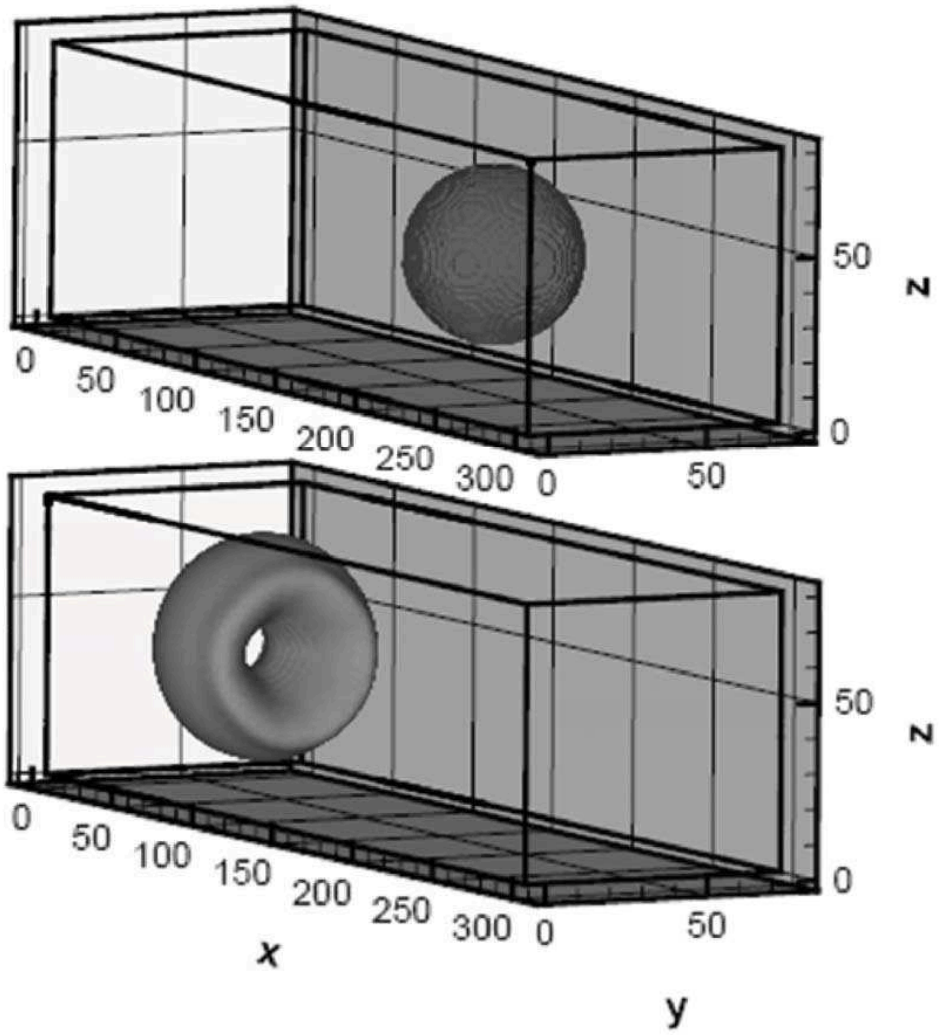

FIG. 8: Density iso-surfaces of a low density bubble at $t = 0.0$, 0.1, respectively.

Acknowledgments

This work is supported by the Science Foundations of LCP and CAEP [under Grant Nos. 2009A0102005, 2009B0101012], National Basic Research Program (973 Program) [under Grant No. 2007CB815105], National Natural Science Foundation [under Grant Nos. 10775018, 10702010] of China.

---

[1] S. Succi, *The Lattice Boltzmann Equation for Fluid Dynamics and Beyond,* Oxford University Press, New York(2001).

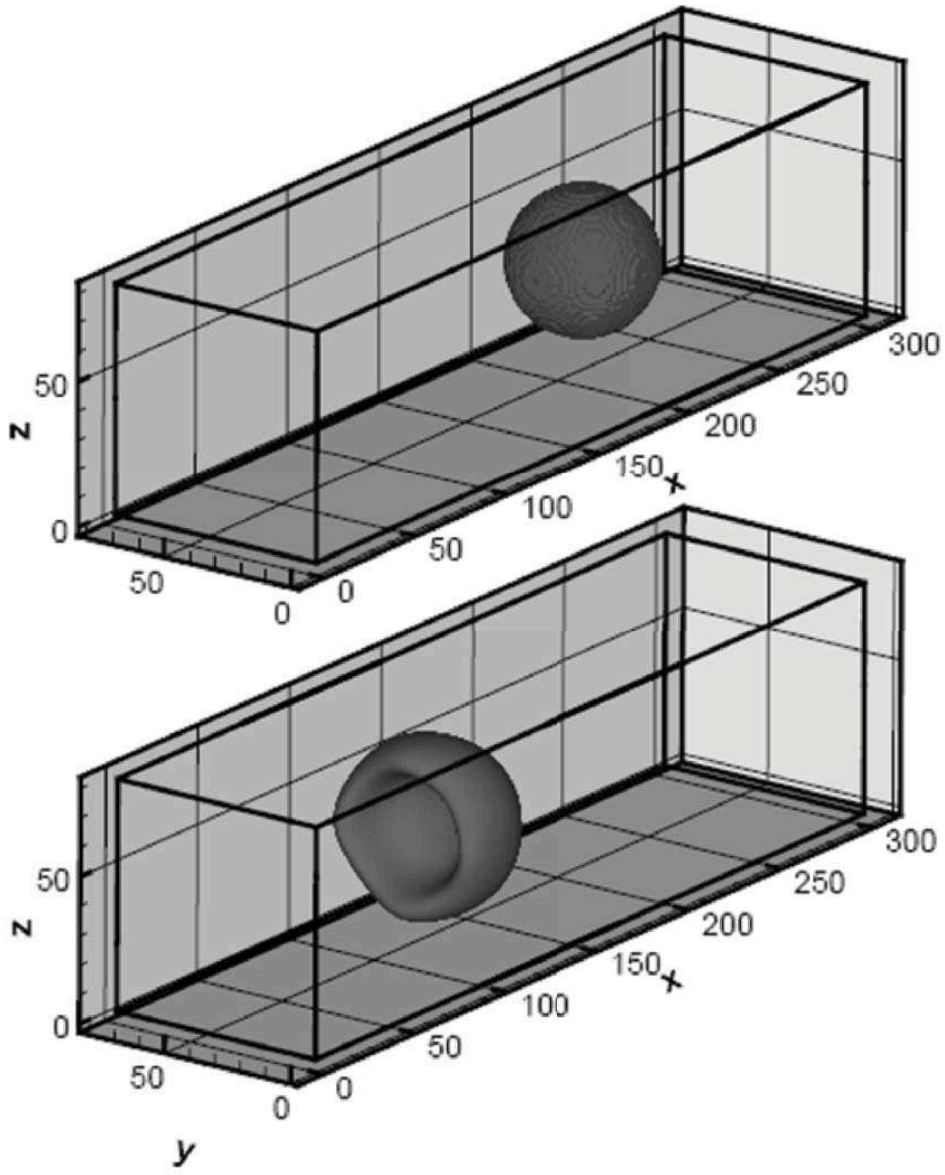

FIG. 9: Density iso-surfaces of a high density bubble at $t = 0.0$, 0.1, respectively.

[2] X. Shan, H. Chen, Phys. Rev. E **47** (1993) 1815; Phys. Rev. E **49** (1994) 2941.

[3] A.G. Xu, G. Gonnella, and A. Lamura, Phys. Rev. E **74** (2006) 011505; Phys. Rev. E **67** (2003) 056105; Physica A **331** (2004) 10; Physica A **344** (2004) 750; Physica A **362** (2006) 42; A.G. Xu, Commun. Theor. Phys. **39** (2003) 729.

[4] S.Chen, H.Chen, D.Martinez, and W.Matthaeus, Phys. Rev. Lett., **67** (1991) 3776.

[5] S.Succi, M.Vergassola and R.Benzi, Phys. Rev. A, **43** (1991) 4521.

[6] G.Breyiannis and D.Valougeorgis, Phys. Rev. E, **69** (2004) 065702(R).

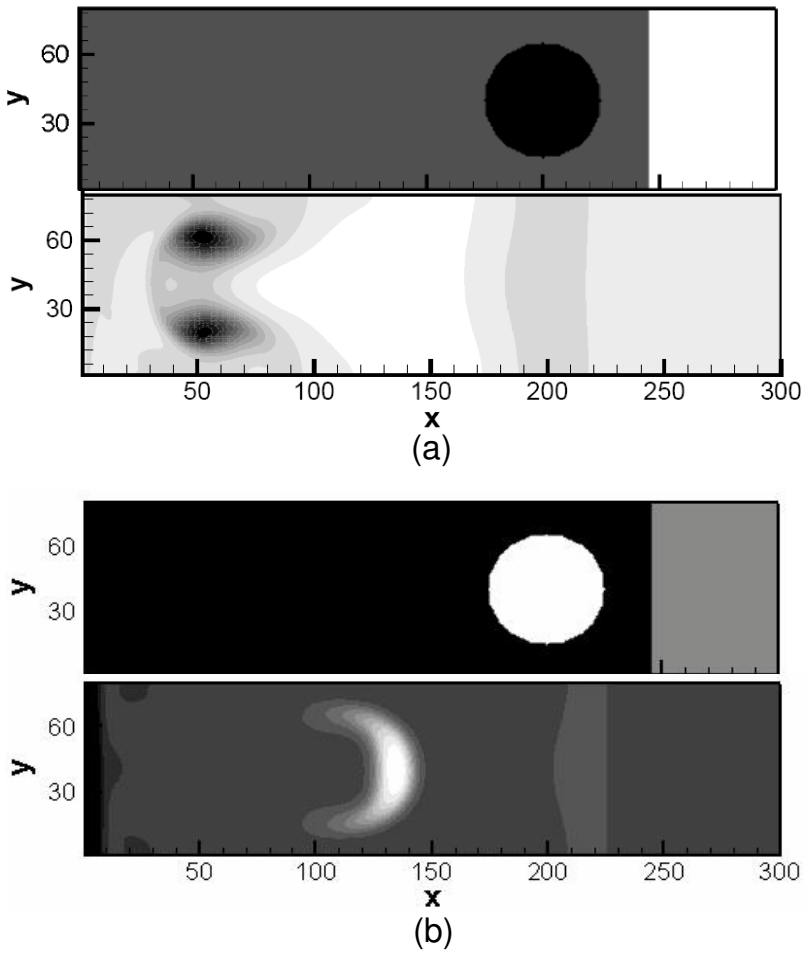

FIG. 10: Density contours on section $z = 40$ at $t = 0.0$, 0.1. (a) and (b) correspond to the processes of Figure 8 and Figure 9. From black to white, the density value increases.

[7] A. Gunstensen and D.H. Rothman, J. Geophy. Research **98** (1993) 6431.

[8] Q. J. Kang, D. X.Zhang, and S. Y.Chen, Phys. Rev. E, **66** (2002) 056307.

[9] Y. Chen, H. Ohashi, and M. Akiyama, J. Sci. Comp. **12** (1997) 169.

[10] S.X. Hu, G.W. Yan, W.P. Shi, Acta Mech. Sinica (English Series) **13** (1997) 218.

[11] G.W. Yan, Y.S. Chen, S.X. Hu, Phys. Rev. E **59** (1999) 454.

[12] W.P. Shi, W. Shyy, R. Mei, Numer. Heat Transfer, Part B **40** (2001) 1.

[13] T. Kataoka, M. Tsutahara, Phys. Rev. E **69** (2004) 056702.

[14] F. Tosi, S. Ubertini, S. Succi, H. Chen, I.V. Karlin, Math. Comput. Simul. **72** (2006) 227.

[15] V. Sofonea, A. Lamura, G. Gonnella, A. Cristea, Phys. Rev. E **70** (2004) 046702.

[16] X.F. Pan, A.G. Xu, G.C. Zhang, and S. Jiang, Int. J. Mod. Phys. C **18** (2007) 1747.

[17] Y.B. Gan, A.G. Xu, G.C. Zhang, X.J. Yu, and Y.J. Li, Physica A **387** (2008) 1721.

[18] F. Chen, A.G. Xu, G.C. Zhang, Y.B. Gan, T. Cheng, and Y.J. Li, Commun. Theor. Phys., **52** (2009) 681.

[19] R. A. Brownlee, A. N. Gorban, J. Levesley, Phys. Rev. E **75** (2007) 036711.

[20] F. Chen, A.G. Xu, G. C. Zhang, Y. J. Li and S. Succi, Europhys. Lett., (in press) [arXiv:1004.5442].

[21] M. Watari, M. Tsutahara, Physica A **364** (2006) 129.

[22] Q. Li, Y.L. He, Y. Wang, G.H. Tang, Physics Letters A **373** (2009) 2101.

[23] P. Bhatnagar, E. P. Gross, and M. K. Krook, Phys. Rev. **94** (1954) 511.

[24] C. Q. Jin, K. Xu. J. Comput. Phys. **218** (2006) 68.

[25] D. X. Fu, Y. W. Ma, X. L. Li, Chinese Phys. Lett. **25** (2008) 188.

[26] J. F. Haas, B. Sturtevant, J. Fluid Nech. **181** (1987) 41.